



OPEN

A theoretical framework for general design of two-materials composed diffractive fresnel lens

Ming-Yen Lin¹, Chih-Hao Chuang², Tzu-An Chou³ & Chien-Yu Chen³✉

Near 100% of diffractive efficiency for diffractive optical elements (DOEs) is one of the most required optical performances in broadband imaging applications. Of all flat DOEs, none seems to interest researchers as much as Two-Materials Composed Diffractive Fresnel Lens (TM-DFL) among the most promising flat DOEs. An approach of the near 100% of diffractive efficiency for TM-DFL once developed to determine the design rules mainly takes the advantage of numerical computation by methods of mapping and fitting. Despite a curved line of near 100% of diffractive efficiency can be generated in the Abbe and partial dispersion diagram, it is not able to analytically elaborate the relationship between two optical materials that compose the TM-DFL. Here, we present a theoretical framework, based on the fundamentals of Cauchy's equation, Abbe number, partial dispersion, and the diffraction theory of Fresnel lens, for obtaining a general design formalism, so to perform the perfect material matching between two different optical materials for achieving the near 100% of diffractive efficiency for TM-DFL in the broadband imaging applications.

Previous researches on diffractive Fresnel lens (DFL)

In the thinning of optical lenses, following the principle of Equal Optical Path Difference, the surface relief of a spherical lens with radius R and refractive index $n(\lambda)$ is processed to construct a Diffractive Fresnel Lens (DFL) with multiple concentric Fresnel Zone (FZ) on the surface^{1–11}, as shown in Fig. 1.

Usually, exploiting the $2p\pi$ phase (where p is a positive integer) as the Equal Optical Path Difference is the way to configure a diffractive Fresnel lens (DFL)^{12–18}. The so-called DFL is generally referred to $p=1$. According to the basic diffractive optics theory of DFL presented by Dale A. Buralli¹², as shown in Fig. 1, the radial FZ structure possesses the following relations.

$$r_i^2 = 2i\lambda_0 f_0 \quad (1)$$

$$\Lambda_i = \frac{\lambda_0 f_0}{r_i} \quad (2)$$

$$h = \frac{\lambda_0}{n(\lambda_0) - 1} \quad (3)$$

$$D = 2r_{max} \quad (4)$$

where r_i is the i -th FZ radius, f_0 is the design focal length, λ_0 is the design wavelength, Λ_i is the spacing between the i -th FZ and the $i+1$ -th FZ, h is the FZ height, D is the FZ diameter, and r_{max} is the outermost FZ radius.

Due to the dispersion, generally the parallel incident white light with different wavelengths, ranging from 400 to 700 nm, is focused by DFL at different focal points on the optical axis. The optical power varies linearly with the wavelength of the incident light, as shown in Fig. 2, where f_R , f_G , and f_B presenting the focal points focused by the red, green, and blue light respectively.

¹3D Interaction & Display Association, Taipei, Taiwan, ROC. ²Graduate Institute of Photonics and Optoelectronics, National Taiwan University, Taipei 10617, Taiwan, ROC. ³Graduate Institute of Color and Illumination Technology, National Taiwan University of Science and Technology, Taipei 10607, Taiwan, ROC. ✉email: chencyue@mail.ntust.edu.tw

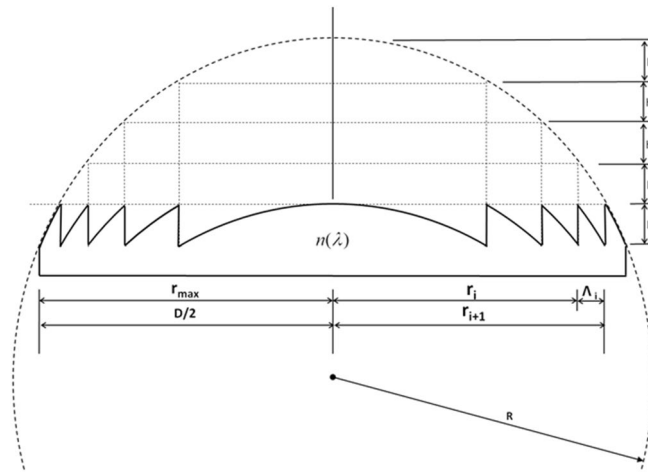


Figure 1. Conventional thinning process of a diffractive Fresnel lens (DFL) based on the principle of equal optical path difference.

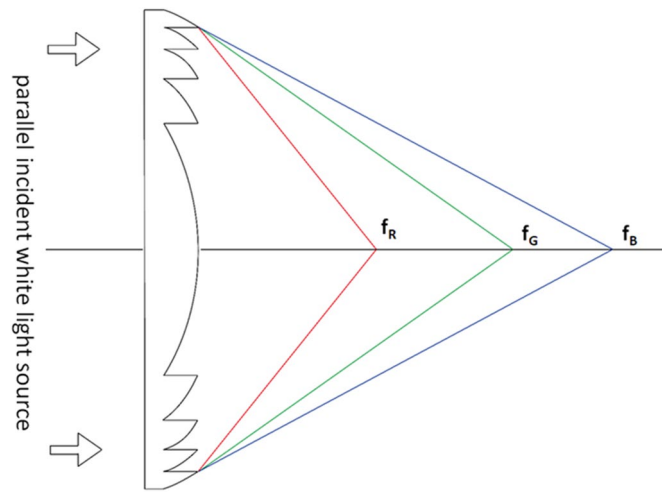


Figure 2. Optical power of a DFL as a function of the wavelength of the incident light.

Furthermore, according to the above-mentioned theory of DFL¹², the diffraction focus and efficiency of a light source with a single wavelength can be determined by the following equations.

$$f = \frac{\lambda_0 f_0}{\lambda m} \tag{5}$$

$$\eta = \left[\frac{\sin\pi(\alpha - m)}{\pi(\alpha - m)} \right]^2 \tag{6}$$

$$\alpha = \frac{\lambda_0 n(\lambda) - 1}{\lambda n(\lambda_0) - 1} \tag{7}$$

where λ_0 is the design wavelength, f_0 is the design focal length, λ is the wavelength, f is the focal length, m is the diffracted order, η is the diffractive efficiency, α is the detuning factor, $n(\lambda)$ is the refractive index of DFL as a function of wavelength λ , and $n(\lambda_0)$ is the refractive index at $\lambda = \lambda_0$.

For instance, the wavelength dependent diffractive efficiency $\eta(\lambda)$ of the optical materials of PMMA (Microchem 495 PMMA resist¹⁹) is calculated by Eqs. (3), (6), and (7) for the design wavelength at $\lambda_0 = 0.587 \mu\text{m}$, FZ height at $h = 1.17 \mu\text{m}$, and the diffracted order at $m = 1, 2,$ and 3 , as shown in Fig. 3.

The calculation results reveal that most of the diffraction energy transmitted from the white incident light focused in the diffracted order at $m = 1$ and only a small portion of the diffraction energy contributed to the

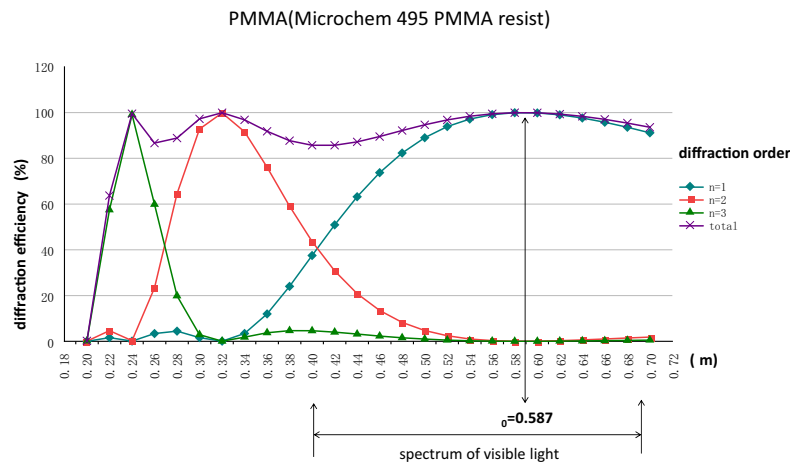


Figure 3. Diffractive efficiency $\eta(\lambda)$ of PMMA as a function of the incident light wavelength λ at diffraction order $m = 1, 2$, and 3 .

diffracted order at $m = 2, 3$, while the rest of the energy from the higher diffracted order being not considered because of the less contribution to the diffractive efficiency. Furthermore, in the spectrum of visible light, according to Eqs. (6) and (7), 100% diffractive efficiency can only be achieved in conditions of the diffracted order at $m = 1$, $\lambda = \lambda_0 = 0.587 \mu\text{m}$, and $\alpha = 1$. Equation (6) describes how the diffractive efficiency drops off when the incident wavelength λ deviates away from the design wavelength λ_0 . More practically, the overall diffractive efficiency is generally evaluated with the mean value of spectrum distribution, as following equations.

$$\bar{\eta}_m = \frac{1}{\lambda_2 - \lambda_1} \int_{\lambda_1}^{\lambda_2} \eta_m(\lambda) d\lambda \quad (8)$$

$$\bar{\eta}_T = \sum_{m=1}^{\infty} \bar{\eta}_m \quad (9)$$

where $\bar{\eta}_m$ is the averaged diffractive efficiency in the diffracted order at m and $\bar{\eta}_T$ is the total averaged diffractive efficiency. For the parallel incident white light source, substituting the wavelength at $\lambda_1 = 0.4 \mu\text{m}$ and $\lambda_2 = 0.7 \mu\text{m}$ into Eqs. (8) and (9), $\bar{\eta}_1 \sim 85.2\%$, $\bar{\eta}_2 \sim 8.2\%$, and $\bar{\eta}_3 \sim 1.2\%$ are obtained in the diffracted order at $m = 1$, $m = 2$ and $m = 3$ respectively.

Consequently, the total diffractive efficiency from $m = 1$ to $m = 3$ comes up with $\bar{\eta}_T = 94.8\%$. In other words, there is still a certain portion of the incident light transmitted to other higher diffracted order ($m > 3$). For the diffracted order at $m = 1$ and $h = 1.17 \mu\text{m}$, about 15% of the incident light energy is disappeared. As a result, such light becomes the stray light and eventually deteriorates the imaging quality of DFL.

A solution to make up for the energy loss in the first diffracted order was first presented by Kenneth J. Weible in 1999²⁰. In their research result, a blazed grating, composed of two optical materials, including glass (Schott BaF52 glass) and PC (polycarbonate), was proposed to improve the diffractive efficiency for the diffracted order at $m = 1$ (i.e. $\alpha = 1$) by exploiting the refractive index difference $\Delta n(\lambda) = n_1(\lambda) - n_2(\lambda)$ being proportional to wavelength λ . When the refractive index difference satisfies $\Delta n(\lambda)/\lambda = \text{constant}$ at all wavelengths λ in the spectrum of visible light, all the incident light energy in the higher diffracted order is all transferred into the first diffracted order, as to achieve the objective of 100% diffractive efficiency. Furthermore, B. H. Kleemann mentioned the design concepts for the blazed grating composed of two optical materials in 2008²¹ and particularly named such structure as Common depth EA-DOEs. In contrast to the term ‘‘Common depth’’, a singlet DFL composed of two optical materials is called Two-Materials Composed Diffractive Fresnel Lens (TM-DFL) in this study.

According to Kenneth’s research²⁰, two transparent optical materials of glass²² and PC²³, as shown in Fig. 4a and b, are used for explaining the difference in the diffractive efficiency between a Single-Material Composed Diffractive Fresnel Lens (SM-DFL), i.e. the conventional DFL, and TM-DFL. For SM-DFL, the average diffractive efficiency $\bar{\eta}_1$ 84.9% is calculated by Eqs. (6), (7), and (8) for the diffracted order at $m = 1$ and the incident wavelength at $\lambda = 400\text{--}700 \text{ nm}$, as shown in Fig. 4c. Besides, for TM-DFL, the diffractive efficiency $\bar{\eta}_1 = 94.3\%$, as shown in Fig. 4d, is obtained by the same calculations above with a modified tuning factor α in Eq. (10) which contains the refractive index $n_2(\lambda)$ and $n_2(\lambda_0)$ of the second material.

$$\alpha = \frac{\lambda_0}{\lambda} \frac{n_1(\lambda) - n_2(\lambda)}{n_1(\lambda_0) - n_2(\lambda_0)} \quad (10)$$

Although TM-DFL can improve the diffractive efficiency of the conventional SM-DFL, the requirement for $\Delta n(\lambda) \propto \lambda$ is not perfectly satisfied. As a result, it is hard to achieve the theoretical 100% diffractive efficiency.

In fact, Andrew Wood²⁴ indicated that in the case of SM-DFL composed with materials existing in nature, the detuning factor α in Eq. (7) could hardly retain the needs for $\alpha = 1$ when λ deviated away from the design

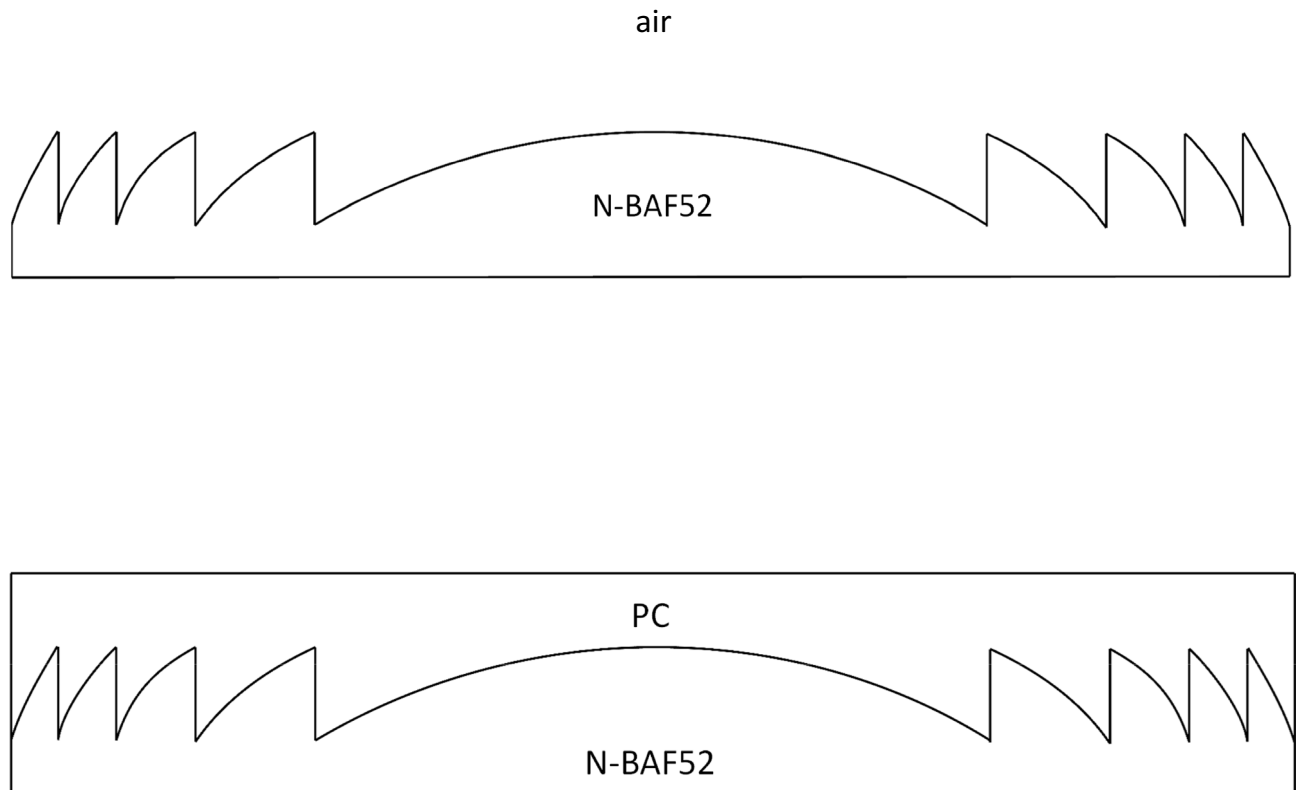


Figure 4. Difference between SM-DFL and TM-DFL. (a) material composed of a SM-DFL (b) material composed of a TM-DFL (c) diffraction efficiency of SM-DFL at $m = 1$ (d) diffraction efficiency of TM-DFL at $m = 1$.

wavelength λ_0 . Moreover, as previously described, the regular materials, i.e. glass and PC, found by Kenneth J. Weible²⁰ were able to increase the average diffractive efficiency from 85 to 94%, but it still required more effort to realize the theoretical 100% diffractive efficiency.

Latest works on the optical design of TM-DFL: a numerical framework for the design of broadband DOEs. To overcome the above-mentioned problems, Daniel Werdehausen in 2019²⁵ proposed to use dispersion-engineered nanocomposites for artificially generating a refractive index difference $\Delta n(\lambda)$ to satisfy the requirement for $n(\lambda) \propto \lambda$. According to this definition²⁵, the so-called nanocomposites are produced by adding a proper volume fraction of nanoparticles with a diameter smaller than 5 nm, such as Diamond, ZrO_2 , TiO_2 , ITO (indium tin oxide), and AZO (aluminum-doped zinc oxide) (presented as green stars), to the existing polymeric materials, such as PMMA (poly(methyl methacrylate)), COP (cyclic olefin copolymer), PC (polycarbonate), and PS (polystyrene) (presented as blue stars), to adjust the optical parameters of materials n_d , v_d , and $P_{g,F}$. Though such new n_d , v_d , and $P_{g,F}$ (presented as orange points) do not exist in nature, they can be tailored within a certain range (presented as pink area) in both the Abbe diagram and partial dispersion diagram, as respectively shown in Fig. 4a and b²⁵. For instance, by adding TiO_2 nanoparticles with different volume fraction to the polymeric material PC, the distribution of n_d - v_d can extend to cover a region in $17 < v_d < 28$ and $1.6 < n_d < 1.85$ while the distribution of $P_{g,F}$ - v_d covers a region in $17 < v_d < 28$ and $0.58 < P_{g,F} < 0.65$.

Furthermore, the same research team in 2020²⁶ proposed a design method of mapping and fitting based on the numerical computation for matching the material refractive index of TM-DFL to achieve the light diffractive efficiency higher than 99.9%. According to DOEs' phase profiles change across the different dispersion regimes²⁶, the material parameters of material 1 (Mat.1) are first selected and set at $n_{d,1} = 1.8$, $v_{d,1} = 60$, and $P_{g,F,1} = 0.55$. By the method of mapping, the material parameters $n_{d,2}$, $v_{d,2}$, and $P_{g,F,2}$ of material 2 (Mat. 2) are discretely varied to calculate the distribution of the average diffractive efficiency $\bar{\eta}$ in the Abbe diagram. Similarly, the distribution of the average diffractive efficiency $\bar{\eta}$ in the partial dispersion diagram is calculated and drawn. For later discussion, the diffractive efficiency $\bar{\eta}(n_{d,2}, v_{d,2})_{mat1}$ and $\bar{\eta}(P_{g,F,2}, v_{d,2})_{mat1}$ are defined as a function of $(n_{d,2}, v_{d,2})$ and $(P_{g,F,2}, v_{d,2})$ respectively. The subscript Mat.1 in both function $\bar{\eta}$ stands for the values of the material parameters $n_{d,1}$, $v_{d,1}$, and $P_{g,F,1}$ of Mat.1 being fixed as a constant.

The major feature of the mapping method is to discretely modulate $n_{d,2}$, $v_{d,2}$, $P_{g,F,2}$ of Mat. 2 in a large region to calculate and set up both diffractive efficiency map of $\bar{\eta}(n_{d,2}, v_{d,2})_{mat1}$ and $\bar{\eta}(P_{g,F,2}, v_{d,2})_{mat1}$, so to find the black dotted curved lines where the calculated $n_{d,2}$, $v_{d,2}$, $P_{g,F,2}$ of Mat. 2 matches to the selected $n_{d,1}$, $v_{d,1}$, and $P_{g,F,1}$ of Mat.1 for achieving the near 100% diffractive efficiency. Hereafter, the black dotted curved line in $\bar{\eta}(n_{d,2}, v_{d,2})_{mat1}$ is named as Abbe characteristic curve of the near 100% of diffractive efficiency, or Abbe characteristic curve in brief, while the other one in $\bar{\eta}(P_{g,F,2}, v_{d,2})_{mat1}$ is named as partial dispersion characteristic curve of the near

100% of diffractive efficiency, or partial dispersion characteristic curve in brief. Finally, the most suitable material parameters $n_{d,2}$, $v_{d,2}$, and $P_{g,F,2}$ can be determined by comparing the producible nanocomposites for completing the optimal match of parameters in two nanocomposite materials.

Furthermore, applying the mathematical fitting to the Abbe characteristic curve, a natural exponential function is obtained, as below.

$$n_{d,2}(v_{d,2}) = a(1 - e^{b(v_{d,2}-c)^{1/3}}) \quad (11)$$

where $a = 1.839$, $b = 0.9919$, and $c = 0.8782$. Note that these values are determined only for $n_{d,1} = 1.8$, $v_{d,1} = 60$, and $P_{g,F,1} = 0.55$. To acquire the general relationship between a , b , c , and the material parameters of MAT.1, ten of the Abbe characteristic curves with different values of $n_{d,1}$, ranging from 1.5 to 2.0, are used to fit to obtain the $n_{d,1}$ dependence of a , b , and c as below.

$$a(n_{d,1}) = 1.071n_{d,1} - 0.07825 \quad (12)$$

$$b(n_{d,1}) = \frac{0.9555}{n_{d,1}^4} - 0.07825 \quad (13)$$

$$c(n_{d,1}) = 53.59\sqrt{n_{d,1}} - 16.59n_{d,1} - 41.17 \quad (14)$$

However, the fitting to the partial dispersion characteristic curve, is not discussed²⁶.

Major issues left by latest works. In summary, to achieve the optical parameters match for two nanocomposite materials in TM-DFL, the above-mentioned design method of mapping and fitting by the numerical computation²⁶ confronts the following issues.

- (1) The methods of mapping can obtain a single Abbe characteristic curve and partial dispersion characteristic curve through a big volume of numerical computations at a time while losing efficiency and accuracy.
- (2) The fitting method can describe the Abbe characteristic curve as Eq. (11) which is a function of $n_{d,1}$ in a special form of a natural exponential function with 1/3 power. In addition to the fitting accuracy or error, it is not a general equation for the analytical evaluation of the system. The so-called “analytical evaluation” refers to analyze the variance in the entire system caused by the parameter variation without using massive numerical computations. In other words, it is a qualitative and quantitative way to get insight into the general physical behaviors of a system by theoretical formulas.
- (3) Three coefficients a , b , and c of the Abbe characteristic curve merely contains $n_{d,1}$ of Mat.1 without any further relation with $v_{d,1}$ and $P_{g,F,1}$ of Mat.1.
- (4) There is no fitting applied to the partial dispersion characteristic curve for the analytical evaluation on the relationship among parameters, i.e. ($n_{d,1}$, $v_{d,1}$, and $P_{g,F,1}$) and ($n_{d,2}$, $v_{d,2}$, and $P_{g,F,2}$) between two materials.

New method: a theoretical framework for general design formalism. In contrast, we present a new method of analytical evaluation based on theoretical formulas in this study. More exactly, two characteristic curve formulas of the near 100% of diffractive efficiency are derived from the theories of Cauchy’s equation, Abbe number, and partial dispersion as well as the diffractive theory of Fresnel lens. Besides, to achieve the purposes of the perfect parameters match between two optical materials in TM-DFL and the objectives of the general analyses on the optical behavior of TM-DFL, it completely solves the above-mentioned disadvantages of the numerical computation-based methods of mapping and fitting.

For the optical theory of DFL, the previous theoretical Eqs. (1)–(9) completely describe the relationship among the diffractive efficiency, the wavelength of the incident light, and material refractive index, where Eqs. (1)–(4) provide the design of the geometric shape of Fresnel lens, Eqs. (5)–(7) provide the focal length and diffractive efficiency after the incident light interactive with DFL, and Eqs. (8)–(9) provide the overall evaluation of diffractive efficiency.

For DFL, 2π phase shift is the necessary condition for reaching 100% diffractive efficiency which can be acquired when $h\Delta n(\lambda_0) = \lambda_0$, where h is the FZ height, $\Delta n(\lambda_0) = n(\lambda_0) - 1$ is the refractive index difference, $n(\lambda_0)$ is the material refractive index of DFL at $= \lambda_0$, λ is the wavelength of the incident light, and λ_0 is the design wavelength. Further, “1” in the Δn is the refractive index of air. That is, the incident light directly contacts the air after going through DFL. Since the refractive index of air is almost irrelevant to λ , it is no way to satisfy the condition $\Delta n \propto \lambda$. Consequently, the diffractive efficiency drops off significantly when λ deviating away from λ_0 . Therefore, TM-DFL is used to effectively overcome the efficiency issue caused by the refractive index of air. For this purpose, Eq. (3) is modified as below to generate a 2π phase shift when TM-DFL is used to replace DFL.

$$h = \frac{\lambda_0}{n_1(\lambda_0) - n_2(\lambda_0)} \quad (15)$$

where $n_1(\lambda_0)$ and $n_2(\lambda_0)$ are the value of two material refractive indexes in TM-DFL at $= \lambda_0$.

Moreover, the detuning factor α in Eq. (7) also needs a modification as in Eq. (10). Practically, the two optical materials used for TM-DFL have to satisfy the following requirements, including (1) optically transparent in the visible spectrum, (2) practical in mass production, and (3) $\Delta n(\lambda) \propto \lambda$. As the transparent materials existing in nature can hardly satisfy all the above conditions, especially for (3). Consequently, an optical material with

an artificially tailorable refractive index, such as nanocomposite, is necessary for the realization of TM-DFL. The core of this research is to build up a theoretical foundation for the design of TM-DFL with the near 100% of diffractive efficiency by connecting theories of Cauchy's equation, Abbe number, partial dispersion, and the diffractive theory of Fresnel lens all together to derive the equation of Abbe characteristic curve and partial dispersion characteristic curve as below.

Solution for coefficients of Cauchy's equation. In general, the refractive index $n(\lambda)$ of transparent optical materials in the spectrum of visible light can be calculated by Cauchy's Eq. (16).

$$n(\lambda) = A + \frac{B}{\lambda^2} + \frac{C}{\lambda^4} \quad (16)$$

where $n(\lambda)$ is the refractive index depending on the light wavelength, λ is the wavelength of light in vacuum, and A, B, C are coefficients. Moreover, the dispersion of transparent optical materials can be defined with Abbe number and partial dispersion, as below.

$$v_d = \frac{n_d - 1}{n_F - n_C} \quad (17)$$

$$P_{g,F} = \frac{n_g - n_F}{n_F - n_C} \quad (18)$$

where n_d , n_F , n_C , and n_g are the refractive indices of materials at the wavelengths of the Fraunhofer d, F, C and g spectral lines (referring to wavelength $\lambda_d = 587.56$ nm, $\lambda_F = 486.13$ nm, $\lambda_C = 656.28$ nm, and $\lambda_g = 435.83$ nm). First, n_d , n_F , n_C , n_g and λ_d , λ_F , λ_C , λ_g are substituted into Eq. (16) to obtain the following equations.

$$n_d = A + \frac{B}{\lambda_d^2} + \frac{C}{\lambda_d^4} \quad (19)$$

$$n_F = A + \frac{B}{\lambda_F^2} + \frac{C}{\lambda_F^4} \quad (20)$$

$$n_C = A + \frac{B}{\lambda_C^2} + \frac{C}{\lambda_C^4} \quad (21)$$

$$n_g = A + \frac{B}{\lambda_g^2} + \frac{C}{\lambda_g^4} \quad (22)$$

Coefficients A, B, and C are solved as below.

$$A = n_d - \left(\frac{B}{\lambda_d^2} + \frac{C}{\lambda_d^4} \right) \quad (23)$$

$$B = \frac{1}{b_1 c_2 - b_2 c_1} \frac{n_d - 1}{v_d} (c_2 - c_1 P_{g,F}) \quad (24)$$

$$C = \frac{1}{b_1 c_2 - b_2 c_1} \frac{n_d - 1}{v_d} [-b_2 + b_1 P_{g,F}] \quad (25)$$

where

$$b_1 = \left(\frac{1}{\lambda_F^2} - \frac{1}{\lambda_C^2} \right) \quad (26)$$

$$b_2 = \left(\frac{1}{\lambda_g^2} - \frac{1}{\lambda_F^2} \right) \quad (27)$$

$$c_1 = \left(\frac{1}{\lambda_F^4} - \frac{1}{\lambda_C^4} \right) \quad (28)$$

$$c_2 = \left(\frac{1}{\lambda_g^4} - \frac{1}{\lambda_F^4} \right) \quad (29)$$

Coefficients A, B, C of Cauchy's equation in Eqs. (23)–(25) clearly present the refractive index as a function of n_d , v_d , $P_{g,F}$ and wavelengths of Fraunhofer d, F, C, and g spectral lines.

Derivation of Abbe characteristic curve. As mentioned above, Eq. (6) is a general equation of diffractive efficiency while Eq. (10) defines the detuning factor α of TM-DFL which is a function of refractive index difference $\Delta n(\lambda)$. For all wavelengths in the spectrum of visible light, the FZ height satisfying $\Delta n(\lambda)h=\lambda$ is the key to direct the diffraction energy of all wavelengths toward 100% of diffractive efficiency at the diffracted order $m = 1$. By substituting $\alpha = 1$ and $\lambda_0 = \lambda_d$ into Eqs. (10) and (15) the following equation is obtained.

$$\frac{n_1(\lambda) - n_2(\lambda)}{\lambda} = \frac{n_1(\lambda_d) - n_2(\lambda_d)}{\lambda_d} = \frac{1}{h} \quad (30)$$

By expanding Eq. (30), it obtains

$$n_2(\lambda) = n_1(\lambda) - \frac{\lambda}{h} \quad (31)$$

For TW-FDL, Eqs. (30)–(31) related to the TM-DFL describe the necessary conditions to achieve the near 100% of diffractive efficiency for all wavelengths at $\lambda = 400\text{--}700$ nm and the diffracted order at $m = 1$. According to the definition in Eq. (17), let the Abbe number $v_{d,2}$ of Mat.2 be defined as below

$$v_{d,2} = \frac{n_{d,2} - 1}{n_{F,2} - n_{C,2}} \quad (32)$$

where $n_{d,2}$, $n_{F,2}$, and $n_{C,2}$ are the refractive indices of Mat.2 at the wavelengths of the Fraunhofer d, F, and C spectral lines. Substituting Eq. (31) into Eq. (32), it obtains

$$n_{d,2} = \frac{1 + (n_{FC,1} - \frac{\lambda_{FC} n_{d,1}}{\lambda_d}) v_{d,2}}{1 - \frac{\lambda_{FC}}{\lambda_d} v_{d,2}} \quad (33)$$

where $n_{FC,1} = n_{F,1} - n_{C,1}$, $\lambda_{FC} = \lambda_F - \lambda_C$, and $n_{d,1}$, $n_{F,1}$, and $n_{C,1}$ are the refractive indices of Mat.1 at the wavelengths of the Fraunhofer d, F, and C spectral lines. Following equation is reformed by multiplying $(n_{d,1} - 1)/(n_{d,1} - 1)$.

$$n_{FC,1} = n_{F,1} - n_{C,1} = \frac{n_{d,1} - 1}{\frac{n_{d,1} - 1}{n_{F,1} - n_{C,1}}} = \frac{n_{d,1} - 1}{v_{d,1}} \quad (34)$$

Substituting Eq. (34) into Eq. (33), it obtains

$$n_{d,2} = \frac{1 + \left(\frac{1}{v_{d,1}} - \frac{\lambda_{FC}}{\lambda_d}\right) n_{d,1} v_{d,2} - \frac{v_{d,2}}{v_{d,1}}}{\left(\frac{1}{v_{d,2}} - \frac{\lambda_{FC}}{\lambda_d}\right) v_{d,2}} \quad (35)$$

where $v_{d,1}$ is the Abbe number of Mat.1. Accordingly, both formulas (33) and (35) depict the same Abbe characteristic curves for TM-DFL with the same calculated results. However, formula (35) provides a clearer scope to know how $n_{d,2}$ is affected by $n_{d,1}$ and $v_{d,1}$ of Mat.1. More accurately, formula (35) can be considered as a general formula of $n_{d,2}$ as a function of $v_{d,2}$, $n_{d,1}$, $v_{d,1}$, λ_F , λ_C , and λ_d . A general form of a function of $n_{d,2}$ is defined as below.

$$n_{d,2} \equiv n_{d,2}(n_{d,1}, v_{d,1}, v_{d,2}, \lambda_d, \lambda_F, \lambda_C) \quad (36)$$

Unlike the conventional methods based on numerical computation, formulas (33) and (35) can accurately and immediately calculate and draw the Abbe characteristic curve in the Abbe diagram without the need for numerous numerical computations. The general behavior of $n_{d,2}$ in Eq. (36) will be elaborated in the later discussion.

Derivation of partial dispersion characteristic curve. According to the definition in Eq. (18), let the partial dispersion $P_{g,F,2}$ of Mat.2 be defined as below.

$$P_{g,F,2} = \frac{n_{g,2} - n_{F,2}}{n_{F,2} - n_{C,2}} \quad (37)$$

where $n_{g,2}$, $n_{F,2}$, and $n_{C,2}$ are the refractive indices of Mat.2 at the wavelengths of the Fraunhofer g, F, and C spectral lines. Substituting Eq. (31) into Eq. (37), it obtains

$$P_{g,F,2} = \frac{n_{FC,1} P_{g,F,1} - \frac{\lambda_{gF}}{\lambda_d} n_{d,1,2}}{\frac{n_{d,2} - 1}{v_{d,2}}} \quad (38)$$

where $\lambda_{gF} = \lambda_g - \lambda_F$ and $n_{d,1,2} = n_{d,1} - n_{d,2}$. Similarly, substituting Eq. (34) into Eq. (38), it obtains

$$P_{g,F,2} = \frac{\frac{n_{d,1} - 1}{v_{d,1}} P_{g,F,1} - \frac{\lambda_{gF}}{\lambda_d} (n_{d,1} - n_{d,2})}{\frac{n_{d,2} - 1}{v_{d,2}}} \quad (39)$$

Accordingly, both formulas (38) and (39) depict the same partial dispersion characteristic curves for TM-DFL with the same calculated results. However, formula (39) provides a more clear scope to know how $P_{g,F,2}$ is affected

by $n_{d,1}$, $v_{d,1}$ and $P_{g,F,1}$ of Mat.1. More accurately, formula (39) can be considered as a general formula of $P_{g,F,2}$ since it is a function of $n_{d,1}$, $v_{d,1}$, $P_{g,F,1}$, $n_{d,2}$, $v_{d,2}$, λ_p , λ_g , λ_d . A general form of a function of $P_{g,F,2}$ is defined as below.

$$P_{g,F,2} \equiv P_{g,F,2}(n_{d,1}, v_{d,1}, P_{g,F,1}, n_{d,2}, v_{d,2}, \lambda_d, \lambda_g, \lambda_F) \quad (40)$$

Unlike the conventional methods based on numerical computation, formulas (38) and (39) can accurately and immediately calculate and draw the partial dispersion characteristic curve in the partial dispersion diagram without the need for numerous numerical computations. The general behavior of $P_{g,F,2}$ in formula (39) will be elaborated in the later discussion.

Usually, as mentioned previously, the analytical evaluation is a way to look into the general physical behavior of a system, such as $n_{d,2}$ and $P_{g,F,2}$ in formula (36) and (40), by applying the partial differential to the system at each parameter, such as parameters of optical materials of TM-DFL, so to understand the system response $\Delta n_{d,2}$ and $\Delta P_{g,F,2}$, given as below.

$$\Delta n_{d,2} \cong \frac{\partial n_{d,2}}{\partial n_{d,1}} \Delta n_{d,1} + \frac{\partial n_{d,2}}{\partial v_{d,1}} \Delta v_{d,1} + \frac{\partial n_{d,2}}{\partial v_{d,2}} \Delta v_{d,2} \quad (41)$$

$$\Delta P_{g,F,2} \cong \frac{\partial P_{g,F,2}}{\partial n_{d,1}} \Delta n_{d,1} + \frac{\partial P_{g,F,2}}{\partial v_{d,1}} \Delta v_{d,1} + \frac{\partial P_{g,F,2}}{\partial P_{g,F,1}} \Delta P_{g,F,1} + \frac{\partial P_{g,F,2}}{\partial n_{d,2}} \Delta n_{d,2} + \frac{\partial P_{g,F,2}}{\partial v_{d,2}} \Delta v_{d,2} \quad (42)$$

Clearly, It is no necessary to apply the same process of partial differential to both $n_{d,2}$ and $P_{g,F,2}$ against the light wavelength λ_d , λ_p , λ_c , and λ_g because it is no reason to change the definition of Fraunhofer line.

In summary, in contrast to the conventional method²⁶, formulas (33), (35), (38), and (39) presented in this study can obtain the Abbe and partial dispersion characteristic curves of TM-DFL without numerous computations. Further, an analytical evaluation for getting more insight into the general physical behavior of TM-DFL is elaborated on below.

Results

Hereafter, based on an example of TW-DFL²⁶, we first present a quantitative result in comparison with the one obtained by the conventional method.

According to the example, the optical parameters of Mat.1 are first selected and set to $n_{d,1} = 1.8$, $v_{d,1} = 60$, and $P_{g,F,1} = 0.55$. Then, by the numerical computation based mapping method, the Abbe and partial dispersion diagrams are produced to generate the Abbe and partial dispersion characteristic curves. Finally, the maximum achieved diffractive efficiency can be found at $\eta = \sim 99.1\%$, $n_{d,2} = 1.7$, $v_{d,2} = 18.4$ for the Abbe characteristic curves, and $\eta = \sim 99.9\%$, $v_{d,2} = 15.2$, $P_{g,F,2} = 0.3$ for the partial dispersion characteristic curves. Meanwhile, the Abbe characteristic curve is fitted by Eq. (11) to obtain the coefficients $a = 1.839$, $b = 0.9919$, $c = 0.8782$.

In contrast, in our studies, the Abbe and partial dispersion characteristic curves are obtained by our formulas (35) and (39) respectively, as shown in Fig. 5a and b. There are two Abbe characteristic curves on the same Abbe diagram shown in Fig. 5a, where the green solid line is our result guaranteed by the near 100% diffractive efficiency at each point on the curve while the yellow dotted line is the fitting result of above-mentioned research²⁶. Apparently, the smaller $v_{d,2}$ the larger difference shows the qualitative difference between the two methods. Also, a quantitative difference of the mean value is calculated to 0.0064. In the industrial measurement of the refractive index, this value of 0.0064 is large enough to be easily measured (note: the measurement precision of the Abbe refractometer in the market is 0.0002). In other words, the mapping and fitting methods cause non-negligible errors. Regarding the partial dispersion characteristic curve depicted on the partial dispersion diagram in Fig. 5b, it is no way to do the analytical comparison since no fitting data provided by the above-mentioned research²⁶.

Discussions

In summary, a theoretical formula-based analytical method is proposed in our studies to improve the disadvantages of the numerical computational-based mapping and fitting method. More definitely, the theory of Cauchy's equation, Abbe number, partial dispersion, and the diffractive theory of Fresnel lens are blended into optically connecting two different nanocomposite materials in TM-DFL for achieving the near 100% diffractive efficiency with all wavelengths in the visible spectrum at the first diffracted order. In addition to perfectly matching optical parameters between two materials without numerous computations, it also satisfies the objective of general analysis for TM-DFL in both quantitative and qualitative evaluations. The major features of the optical behavior of TM-DFL in our study are elaborated below.

Feature 1: The general behavior of $n_{d,2}$ ($v_{d,2}$): dependent on $n_{d,1}$ and $v_{d,1}$ only, but independent on $P_{g,F,1}$. As shown in Fig. 6a, the Abbe characteristic curves of Mat.2 in the Abbe diagram is calculated by formula (35) for $n_{d,2}(v_{d,2})$ at $n_{d,1} = 2.0, 1.9, 1.8, 1.7, 1.6, 1.5$, and $v_{d,1} = 50, 40, 30$. When $v_{d,2}$ is fixed, it shows a feature: the larger $n_{d,1}$, the larger $n_{d,2}$. When $n_{d,1}$ is fixed, $n_{d,2}(v_{d,2})$ is split into a subset of lines at $v_{d,1} = 30, 40, 50$, for showing another feature: the less $v_{d,1}$, the larger $n_{d,2}$. Apparently, the Abbe characteristic curves of Mat.2 is nothing to do with $P_{g,F,1}$ because $P_{g,F,1}$ is not included in formula (35).

Feature 2: the general behavior of $P_{g,F,2}$ ($v_{d,2}$): dependent on $P_{g,F,1}$ and $v_{d,1}$ only, but independent on $n_{d,1}$. The partial dispersion characteristic curve of Mat.2 in the partial dispersion diagram is calculated by formula (39). Despite $n_{d,1}$ being an explicit parameter in formula (39), the final calculation is irrelevant

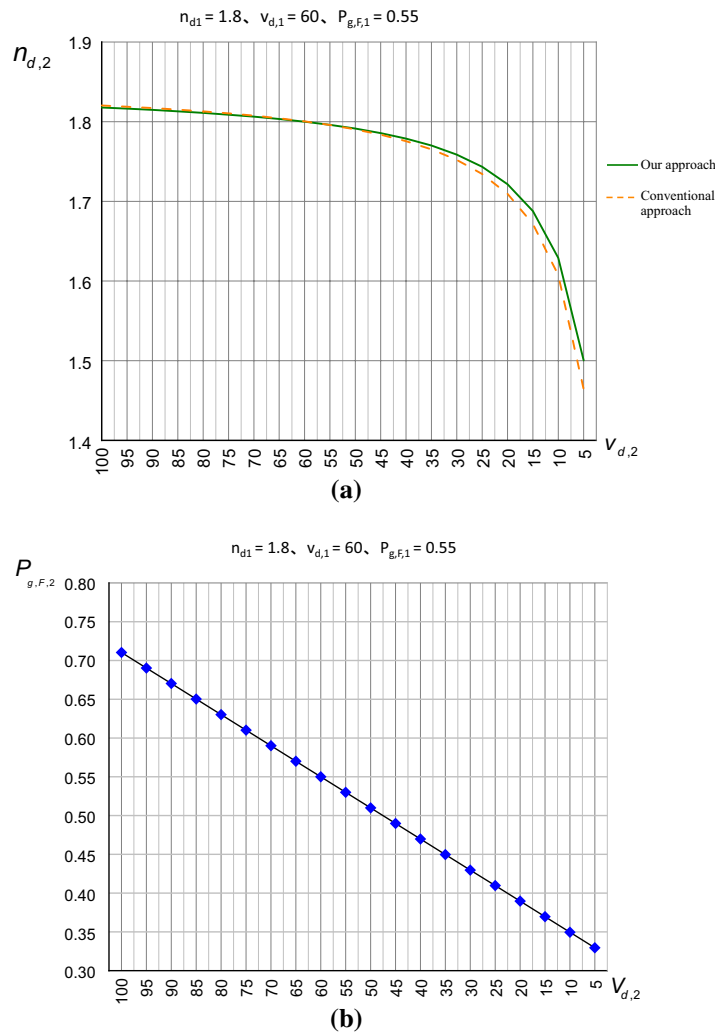


Figure 5. Abbe and partial dispersion characteristic curves. **(a)** our result of Abbe characteristic curve in comparison with the conventional one **(b)** our result of partial dispersion characteristic curves.

to $n_{d,1}$. To analytically prove the independence of $n_{d,1}$, first we need to prove $\Delta P_{g,F,2}/\Delta n_{d,1} = 0$ at all $\Delta n_{d,1}$ and $\Delta P_{g,F,1} = \Delta v_{d,1} = \Delta v_{d,2} = 0$, as below.

By taking the partial derivative of $P_{g,F,2}$ in formula (39) to $n_{d,1}$ and $n_{d,2}$, it obtains

$$\Delta P_{g,F,2} = \frac{\left(\frac{1}{v_{d,1}} P_{g,F,1} - \frac{\lambda_{gF}}{\lambda_d}\right)}{\frac{n_{d,2}-1}{v_{d,2}}} \Delta n_{d,1} + \frac{\left(\frac{\lambda_{gF}}{\lambda_d} - \frac{P_{g,F,2}}{v_{d,2}}\right)}{\frac{n_{d,2}-1}{v_{d,2}}} \Delta n_{d,2} \tag{43}$$

Since $n_{d,2}$ is a function of $n_{d,1}$, taking the partial derivative of $n_{d,2}$ in formula (35) to $n_{d,1}$, it obtains

$$\Delta n_{d,2} = \frac{\frac{1}{v_{d,1}} - \frac{\lambda_{FC}}{\lambda_d}}{\frac{1}{v_{d,2}} - \frac{\lambda_{FC}}{\lambda_d}} \Delta n_{d,1} \tag{44}$$

Substituting Eq. (44) into Eq. (43), it obtains

$$\Delta P_{g,F,2} = \frac{v_{d,2}}{n_{d,2}-1} \left[\left(\frac{1}{v_{d,1}} P_{g,F,1} - \frac{\lambda_{gF}}{\lambda_d}\right) + \left(\frac{\lambda_{gF}}{\lambda_d} - \frac{P_{g,F,2}}{v_{d,2}}\right) \times \frac{\left(\frac{1}{v_{d,1}} - \frac{\lambda_{FC}}{\lambda_d}\right)}{\left(\frac{1}{v_{d,2}} - \frac{\lambda_{FC}}{\lambda_d}\right)} \right] \Delta n_{d,1} \tag{45}$$

The sum of terms in the square brackets in Eq. (45) is always zero after completing the calculation with all parameters in the square brackets. Further, results showing the independency of $n_{d,1}$ by the direct calculation of $P_{g,F,2}(v_{d,2})$ in formula (39), under conditions (1) $n_{d,1} = 2, 1.75, 1.5, v_{d,1} = 50$, and $P_{g,F,1} = 0.7, 0.55, 0.35$ and (2) $n_{d,1} = 2, 1.75, 1.5, v_{d,1} = 30$, and $P_{g,F,1} = 0.7, 0.55, 0.35$, are done and shown in Fig. 6b and c respectively. Accordingly, $P_{g,F,2}(v_{d,2})$ depends on $P_{g,F,1}$ and $v_{d,1}$ only, but not depend on $n_{d,1}$.

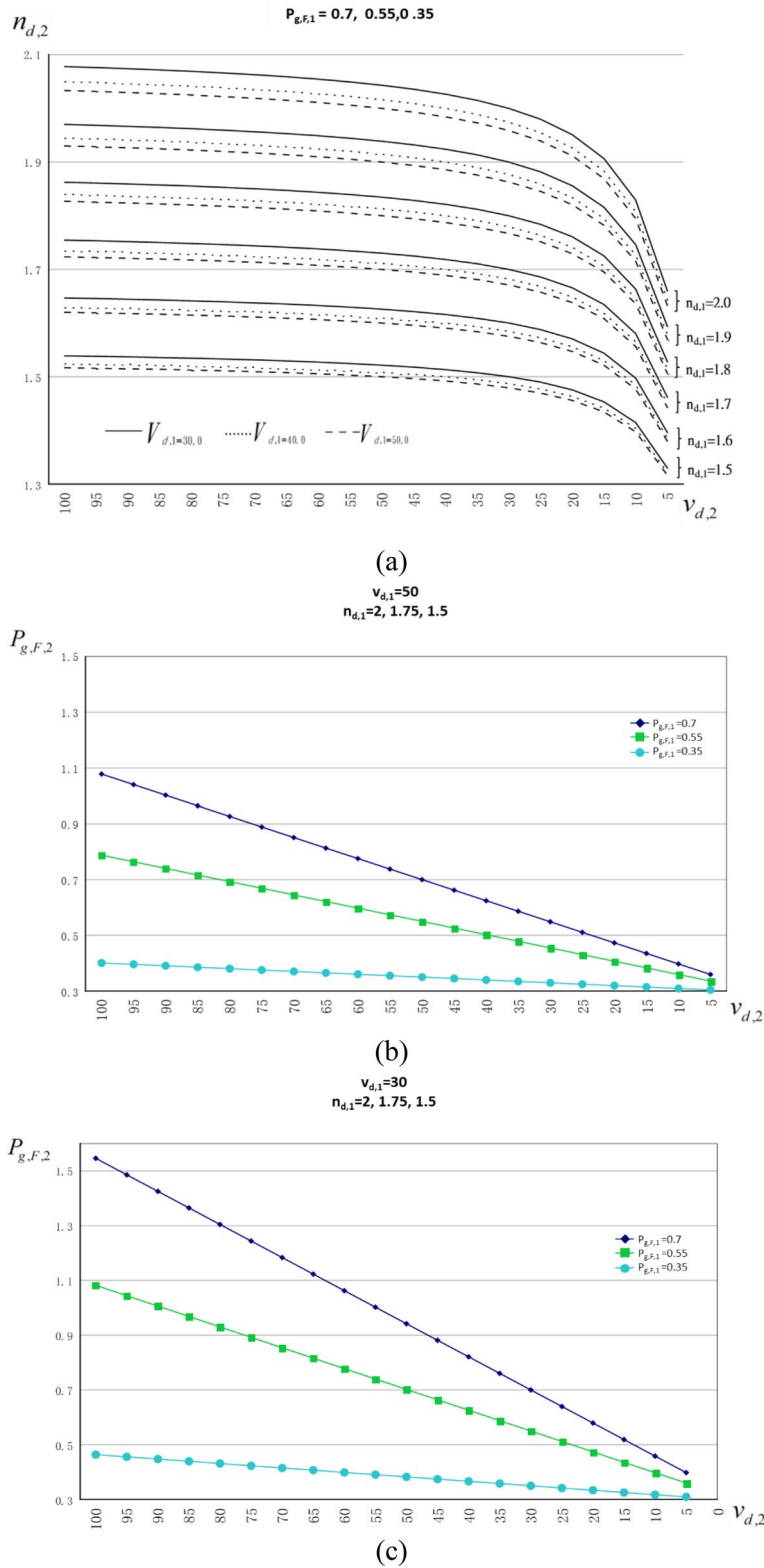


Figure 6. Dependence of $n_{d,2}(v_{d,2})$ and $P_{g,F,2}(v_{d,2})$. (a) $n_{d,2}(v_{d,2})$ is dependent on $n_{d,1}$ and $v_{d,1}$ only but independent on $P_{g,F,1}$, where $n_{d,2}$ is split into a subset of lines at $v_{d,1} = 30, 40, 50$ when $n_{d,1}$ is fixed. (b, c) $P_{g,F,2}(v_{d,2})$ is dependent on $P_{g,F,1}$ and $v_{d,1}$ only but independent on $n_{d,1}$ where $P_{g,F,2}$ is constant when $n_{d,1}$ is varied in the wide range from 2 to 1.5.

MAT. 1		$n_{d,1} = 2.0 - 1.6$								
		$P_{g,F,1} = 50$								
		$V_{d,1} = 0.7$				$V_{d,1} = 0.55$			$V_{d,1} = 0.35$	
i	$V_{d,1}(i)$	$P_{g,F,2}(i)$	$\Delta P_{g,F,2}(i)/\Delta v_{d,2}(i)$	S(i)	$P_{g,F,2}(i)$	$\Delta P_{g,F,2}(i)/\Delta v_{d,2}(i)$	S(i)	$P_{g,F,2}(i)$	$\Delta P_{g,F,2}(i)/\Delta v_{d,2}(i)$	S(i)
MAT. 2										
1	100.0	1.07825	0.00757	0.00757	0.78795	0.00476	0.00476	0.40087	0.00102	0.00102
2	95.0	1.04043	0.00757	0.00757	0.76415	0.00476	0.00476	0.39578	0.00102	0.00102
3	90.0	1.00260	0.00757	0.00757	0.74036	0.00476	0.00476	0.39069	0.00102	0.00102
4	85.0	0.96478	0.00757	0.00757	0.71656	0.00476	0.00478	0.38561	0.00102	0.00102
5	80.0	0.92695	0.00757	0.00757	0.69277	0.00476	0.00476	0.38052	0.00102	0.00102
6	75.0	0.88913	0.00757	0.00757	0.66897	0.00476	0.00476	0.37543	0.00102	0.00102
7	70.0	0.85130	0.00757	0.00757	0.64518	0.00476	0.00476	0.37035	0.00102	0.00102
8	65.0	0.81348	0.00757	0.00757	0.62138	0.00476	0.00476	0.36526	0.00102	0.00102
9	60.0	0.77565	0.00757	0.00757	0.59759	0.00476	0.00476	0.38017	0.00102	0.00102
10	55.0	0.73783	0.00757	0.00757	0.67379	0.00476	0.00476	0.35609	0.00102	0.00102
11	50.0	0.70000	0.00757	0.00757	0.55000	0.00476	0.00476	0.35000	0.00102	0.00102
12	45.0	0.66217	0.00757	0.00757	0.52621	0.00476	0.00476	0.34491	0.00102	0.00102
13	40.0	0.62435	0.00757	0.00757	0.50241	0.00476	0.00476	0.33983	0.00102	0.00102
14	35.0	0.58652	0.00757	0.00757	0.47862	0.00476	0.00476	0.33474	0.00102	0.00102
15	30.0	0.54870	0.00757	0.00757	0.45482	0.00476	0.00476	0.32965	0.00102	0.00102
16	25.0	0.51087	0.00757	0.00757	0.43103	0.00476	0.00476	0.32457	0.00102	0.00102
17	20.0	0.47305	0.00757	0.00757	0.40723	0.00476	0.00476	0.31948	0.00102	0.00102
18	15.0	0.43522	0.00757	0.00757	0.38344	0.00476	0.00476	0.31439	0.00102	0.00102
19	10.0	0.39740	0.00757	0.00757	0.35964	0.00476	0.00476	0.30931	0.00102	0.00102
20	5.0	0.35957	NA	NA	0.33585	NA	NA	0.30422	NA	NA

Table 1. Equivalent results of the local slopes, i.e. $\Delta P_{g,F,2}(i)/\Delta v_{d,2}(i) = S(i) = \text{constant}$, calculated by formula (39) and Eq. (48) show the linearity of $P_{g,F,2}$

Feature 3: $P_{g,F,2}(v_{d,2})$ is linear, i.e. $\Delta P_{g,F,2}/\Delta v_{d,2} = \text{constant}$. By taking the partial derivative of $P_{g,F,2}$ in formula (39) to $v_{d,2}$ and $n_{d,2}$, it obtains

$$\Delta P_{g,F,2} = \frac{P_{g,F,2}}{v_{d,2}} \Delta v_{d,2} + \frac{\frac{\lambda_{gF}}{\lambda_d} v_{d,2}}{n_{d,2}(v_{d,2}) - 1} \Delta n_{d,2} - \frac{P_{g,F,2}}{n_{d,2}(v_{d,2}) - 1} \Delta n_{d,2} \tag{46}$$

Since $n_{d,2}$ is a function of $v_{d,2}$, taking the partial derivative of $n_{d,2}$ in formula (35) to $v_{d,2}$, it obtains

$$\frac{\Delta n_{d,2}}{\Delta v_{d,2}} = \frac{n_{FC,1} - \frac{\lambda_{FC}}{\lambda_d} (n_{d,1} - n_{d,2})}{1 - \frac{\lambda_{FC}}{\lambda_d} v_{d,2}} \tag{47}$$

Using Eq. (34) to replace $n_{FC,1}$ in Eq. (47), then substituting Eq. (47) into Eq. (46), the local slope of $P_{g,F,2}$ is obtained as below.

$$\frac{\Delta P_{g,F,2}}{\Delta v_{d,2}} = \frac{P_{g,F,2}}{v_{d,2}} + \frac{\frac{\lambda_{gF}}{\lambda_d} v_{d,2} - P_{g,F,2}}{n_{d,2} - 1} \times \frac{\frac{n_{d,1}-1}{v_{d,1}} - \frac{\lambda_{FC}}{\lambda_d} (n_{d,1} - n_{d,2})}{1 - \frac{\lambda_{FC}}{\lambda_d} v_{d,2}} \tag{48}$$

Let's move back to the partial dispersion characteristic curve $P_{g,F,2}$ in Fig. 6b. In the previous discussion, we know that $P_{g,F,2}$ depends on $P_{g,F,1}$ and $v_{d,1}$ only, but not depend on $n_{d,1}$. Here, we are going to prove one more feature of the linearity in $P_{g,F,2}$. Referring to Table 1, there are three columns, represented as $P_{g,F,2}(i)$ being a simple form used to replace the term of $P_{g,F,2}(v_{d,2}(i))$, show the data of $P_{g,F,2}$ at different row i which is calculated

by formula (39) with the related material parameters $n_{d,1}$, $v_{d,1}$, $P_{g,F,1}$, $n_{d,2}$, $v_{d,2}$, included in formula (39). Another three columns, represented as $S(i)$, show the data of the local slope directly calculated by Eq. (48) with the related material parameters $n_{d,1}$, $v_{d,1}$, $P_{g,F,2}$, $n_{d,2}$, $v_{d,2}$ included in Eq. (48). Further, more three columns, represented as $\Delta P_{g,F,2}(i)/\Delta v_{d,2}(i)$, show the local slope by directly dividing $\Delta P_{g,F,2}(i) = P_{g,F,2}(i) - P_{g,F,2}(i+1)$ by $\Delta v_{d,2}(i) = v_{d,2}(i) - v_{d,2}(i+1)$. As a result, the quantitative calculations in Table 1 illustrate the linearity of $P_{g,F,2}$ when the equality of $\Delta P_{g,F,2}(i)/\Delta v_{d,2}(i) = S(i) = \text{constant}$ is satisfied at all $i = 1, 19$.

Feature 4: precision (error) of theoretical arithmetic. Further, let's check out how well the material parameters $n_{d,2}$, $P_{g,F,2}$, $v_{d,2}$ in Mat.2 can match up with the predetermined materials $n_{d,1}$, $P_{g,F,1}$, and $v_{d,1}$ in Mat.1 to satisfy the near 100% diffractive efficiency.

According to Cauchy Eqs. (16)–(29), $n_1(\lambda)$ of Mat.1 and $n_2(\lambda)$ of Mat.2 can be calculated by both the predetermined $n_{d,1}$, $P_{g,F,1}$, $v_{d,1}$ and the calculated $n_{d,2}(v_{d,2})$, $P_{g,F,2}(v_{d,2})$ respectively. Then, the detuning factor $\alpha(\lambda)$ is calculated by substituting $n_1(\lambda)$ and $n_2(\lambda)$ into Eq. (10). Finally, according to Eqs. (6) and (8), the diffractive efficiency $\bar{\eta}_m$ is calculated to achieve 99.95% (corresponding to the term “near 100%” used in our research) at the diffracted order $m = 1$ and wavelength from $\lambda_1 = 400$ nm to $\lambda_2 = 700$ nm. Regarding the difference in 0.05% diffractive efficiency, it is reasonable to infer that the error of 0.05% is caused by the miss of the higher approximation terms in the Cauchy Eq. (16). For the exact 100% diffractive efficiency, it can be simply obtained in the following way. Following the same treatments mentioned above, after $n_1(\lambda)$ of Mat.1 being obtained, the FZ height h is calculated first by substituting $n_{d,1}$ and $n_{d,2}$ into Eq. (30), then $n_2(\lambda)$ is obtained according to Eq. (31). Finally, do the same works again to get $\alpha(\lambda) = 1$ and $\eta(\lambda) = 100\%$ at all the wavelength in the visible light spectrum.

Feature 5: the optical behavior of convergence and divergence. In general, for the conventional DFL, the diffractive efficiency is determined by the FZ height h , the refractive index difference Δn , and the incident light wavelength λ while the optical focusing power is determined by the Δn and the curvature $1/R$ of the surface relief of DFL. Let's take up the example used in Fig. 5a and b to further probe into the focusing power related to TM-FDL. As shown in both Figs, the Abbe characteristic curves $n_{d,2}(v_{d,2})$ and the partial dispersion characteristic curve $P_{g,F,2}(v_{d,2})$ are calculated according to formula (35) and (39) respectively. Also, following the previous treatments given in Feature 4 above, an FZ height h is plotted with the respect to $v_{d,2}$, as shown in Fig. 7a, by employing Eq. (30) for matching h with $\Delta n(\lambda)$ at $\lambda = \lambda_d$, i.e. $h(v_{d,2}) = \lambda_d / (n_{d,1} - n_{d,2}(v_{d,2}))$ where $n_{d,1} \equiv n_1(\lambda_d)$ and $n_{d,2} \equiv n_{d,2}(v_{d,2})$, to guarantee the near 100% diffractive efficiency at the first diffracted order and all wavelengths of the incident light in the visible spectrum. Interestingly, there exists a singularity of h at $v_{d,2} = 60$ where $v_{d,2} = v_{d,1}$ and $n_{d,2} = n_{d,1}$. Consequently, the optical behavior of TM-DFL is categorized into three regions as below.

- (1) Transparent region: As shown in Fig. 7a, TM-DFL becomes optical transparent when $v_{d,2} = v_{d,1} = 60$ and $n_{d,2} = n_{d,1} = 1.8$. In other words, both FZ height h and focal length f_0 approach to infinity when TM-FDL is composed of two same optical materials,
- (2) Focusing region: As shown in Fig. 7b and c, TM-DFL is equipped with the focusing power when $v_{d,2} < v_{d,1}$, $h > 0$, $n_{d,2} < n_{d,1}$, and $P_{g,F,2} < P_{g,F,1}$
- (3) Divergent region: As shown in 7(b) and 7(c), TM-DFL is equipped with the divergent power when $v_{d,2} > v_{d,1}$, $h < 0$, $n_{d,2} > n_{d,1}$, and $P_{g,F,2} > P_{g,F,1}$

Conclusions

In our studies, we develop a theoretical framework to obtain a general formalism for the design of TM-DFL in broadband imaging applications. Unlike the existed approach of the numerical computation based methods of mapping and fitting, the optical theories related to Cauchy's equation, Abbe number, and partial dispersion, as well as the diffraction theory of Fresnel lens, have been perfectly blended into a new foundation for working out a TM-DFL with a precise material matching that can theoretically achieve a near 100% diffractive efficiency. The derivation of Equations for the calculations of $n_{d,2}(v_{d,2})$ and $P_{g,F,2}(v_{d,2})$ is elaborated. Also, physical behaviors of $n_{d,2}(v_{d,2})$ and $P_{g,F,2}(v_{d,2})$ are illustrated and proved, including (1) the independence of $P_{g,F,1}$ in $n_{d,2}(v_{d,2})$, (2) the independence of $n_{d,1}$ in $P_{g,F,2}(v_{d,2})$, (3) the linearity and constant slope of $P_{g,F,2}(v_{d,2})$, (4) beyond 0.05% of the theoretical error in the calculation of diffractive efficiency, and (5) the optical behavior of convergence and divergence. We believe that our new approach will be an effective and precise way to achieve a near 100% diffractive efficiency for the design of TM-DFL.

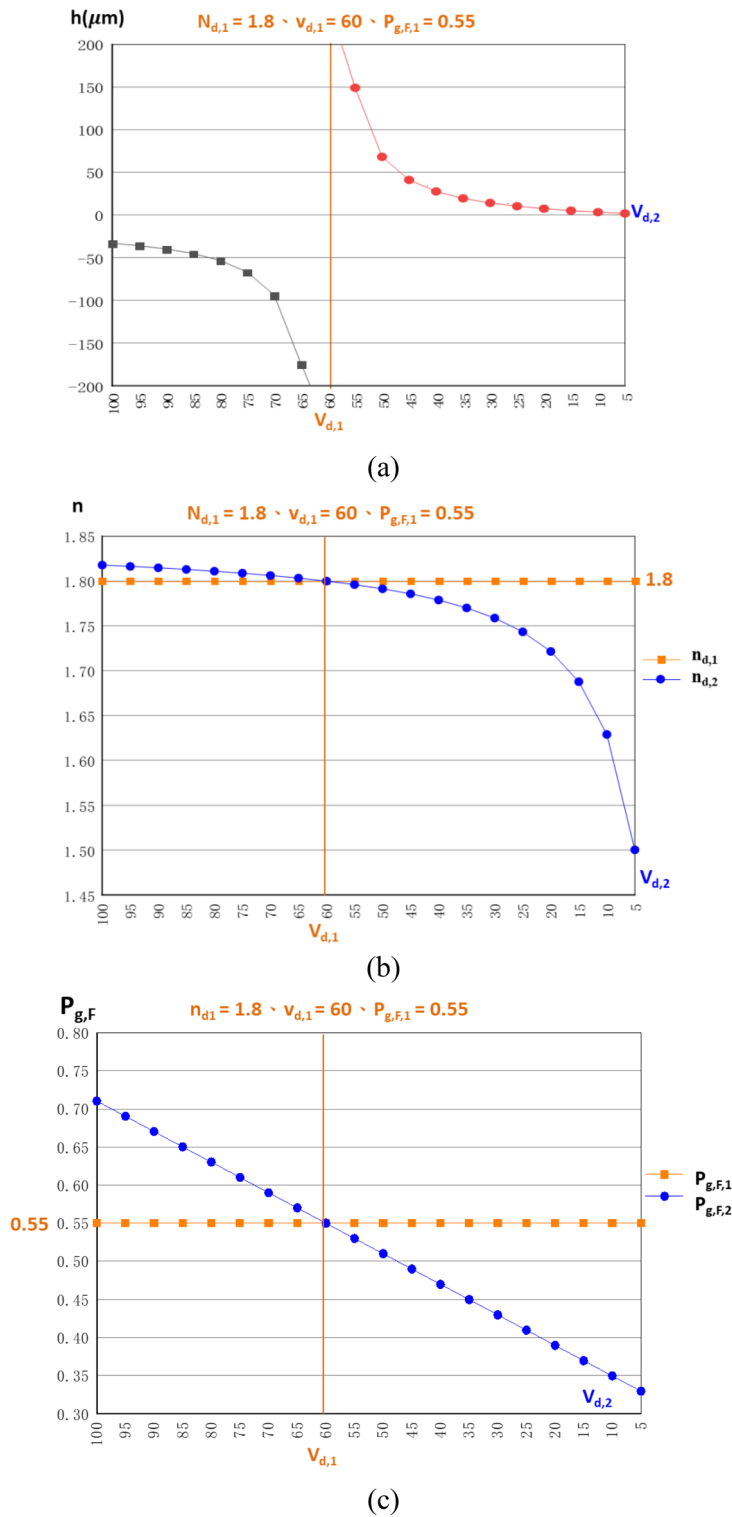


Figure 7. Optical behavior of convergence and divergence in TM-DFL. (a) FZ height h is calculated and plotted as a function of $v_{d,2}$, where TM-DFL becomes optical transparent when $v_{d,2} = v_{d,1} = 60$. (b, c) TM-DFL is equipped with the focusing power when $v_{d,2} < v_{d,1}$, $h > 0$, $n_{d,2} < n_{d,1}$, and $P_{g,F,2} < P_{g,F,1}$, while TM-DFL is equipped with the divergent power when $v_{d,2} > v_{d,1}$, $h < 0$, $n_{d,2} > n_{d,1}$, and $P_{g,F,2} > P_{g,F,1}$.

Received: 21 May 2021; Accepted: 19 July 2021

Published online: 29 July 2021

References

1. Delano, E. Primary aberrations of meniscus Fresnel lenses. *JOSA*. **66**(12), 1317–1320 (1976).
2. Jordan, J. A. *et al.* Kinoform lenses. *Appl. Opt.* **8**, 1883–1887 (1970).
3. Close, D. H. Holographic optical elements. *Opt. Eng.* **14**(5), 145408 (1975).
4. Sweatt, W. C. Describing holographic optical elements as lenses. *JOSA*. **67**(6), 803–808 (1977).
5. Lalanne, P. Waveguiding in blazed-binary diffractive elements. *JOSA A*. **10**, 2517–2520 (1999).
6. Yu, N. *et al.* Light propagation with phase discontinuities: Generalized laws of reflection and refraction. *Science* **334**(6054), 333–337 (2011).
7. Lalanne, P. & Chavel, P. Metalenses at visible wavelengths: Past, present, perspectives. *Laser. Photonics. Rev.* **11**(3), 1600295 (2017).
8. Banerji, S. *et al.* Imaging with flat optics: Metalenses or diffractive lenses?. *Optica*. **6**(6), 805–810 (2019).
9. Engelberg, J. & Levy, U. The advantages of metalenses over diffractive lenses. *Nat. Commun.* **11**(1), 1–4 (2020).
10. O'Shea, D. C. *et al.* *Diffractive Optics: Design, Fabrication And Test* Vol. 62 (SPIE Press, 2004).
11. Kress, B. C. *Field Guide to Digital Micro-Optics* (SPIE, 2014).
12. Buralli, D. A., Morris, G. M. & Rogers, J. R. Optical performance of holographic kinoforms. *Appl. Opt.* **28**(5), 976–983 (1989).
13. Swanson, G. J., Binary optics technology: The theory and design of multi-level diffractive optical elements, *Massachusetts. I. Tech.* (1989).
14. Faklis, D. & Morris, G. M. Spectral properties of multiorder diffractive lenses. *Appl. Opt.* **34**(14), 2462–2468 (1995).
15. Sales, T. R. & Morris, G. M. Diffractive–refractive behavior of kinoform lenses. *Appl. Opt.* **36**(1), 253–257 (1997).
16. Moreno, V. *et al.* High efficiency diffractive lenses: Deduction of kinoform profile. *Am. J. Phys.* **65**(6), 556–562 (1997).
17. Yang, J. *et al.* Chromatic analysis of harmonic Fresnel lenses by FDTD and angular spectrum methods. *Appl. Opt.* **57**(19), 5281–5287 (2018).
18. Werdehausen, D. *et al.* Flat optics in high numerical aperture broadband imaging systems. *J. Opt.* **22**(6), 065607 (2020).
19. Microchem 495 PMMA Resist. https://refractiveindex.info/?shelf=other&book=pmma_resists&page=Microchem495.
20. Weible, K. J. *et al.* Achromatization of the diffraction efficiency of diffractive optical elements. *Proc. SPIE*. **3749**, 378–379 (1999).
21. Kleemann, B. H. *et al.* Design concepts for broadband high-efficiency DOEs. *J. Eur. Opt. Soc. Rapid*. **3**, 08015 (2008).
22. Schott BaF52 Glass. <https://refractiveindex.info/?shelf=organic&book=polycarbonate&page=Sultanova>.
23. Polycarbonate (PC). <https://refractiveindex.info/?shelf=organic&book=polycarbonate&page=Sultanova>.
24. Wood, A. *et al.* Infrared hybrid optics with high broadband efficiency. *Proc. SPIE*. **1**, 5874 (2005).
25. Werdehausen, D. *et al.* Dispersion-engineered nanocomposites enable achromatic diffractive optical elements. *Optica*. **6**(8), 1031–1038 (2019).
26. Werdehausen, D. *et al.* General design formalism for highly efficient flat optics for broadband applications. *Opt. Express*. **28**(5), 6452–6468 (2020).

Acknowledgements

This study was supported by the Ministry of Science and Technology of Taiwan under contract No. 110-2218-E-011-009-MBK & 110-2221-E-011-149.

Author contributions

M.Y.L., C.Y.C. directed the project. M.Y.L. & T.A.C. created the data. M.Y.L. & C.H.C. calculated the data. C.Y.C. optimized calculation processing with M.Y.L. C.H.C. & T.A.C. M.Y.L., C.H.C. & T.A.C. designed and performed the simulation result. All authors contributed to discussions.

Competing interests

The authors declare no competing interests.

Additional information

Correspondence and requests for materials should be addressed to C.-Y.C.

Reprints and permissions information is available at www.nature.com/reprints.

Publisher's note Springer Nature remains neutral with regard to jurisdictional claims in published maps and institutional affiliations.



Open Access This article is licensed under a Creative Commons Attribution 4.0 International License, which permits use, sharing, adaptation, distribution and reproduction in any medium or format, as long as you give appropriate credit to the original author(s) and the source, provide a link to the Creative Commons licence, and indicate if changes were made. The images or other third party material in this article are included in the article's Creative Commons licence, unless indicated otherwise in a credit line to the material. If material is not included in the article's Creative Commons licence and your intended use is not permitted by statutory regulation or exceeds the permitted use, you will need to obtain permission directly from the copyright holder. To view a copy of this licence, visit <http://creativecommons.org/licenses/by/4.0/>.

© The Author(s) 2021